HYDROLOGIC CYCLE AND HEAT TRANSPORT MODELING AND ITS APPLICATION TO THE KANDA RIVER WATERSHED, TOKYO

By

Tsuyoshi Kinouchi

Department of Environment System Management, Fukushima University, Fukushima-Shi, Fukushima, Japan

and

Yangwen Jia

Department of Water Resources, Institute of Water Resources and Hydropower Research, Beijing, China

SYNOPSIS

A physically based distributed hydrological model (WEP model) was coupled with a newly developed model of heat transport in river water to simulate watershed-scale hydrological and heat transport processes and the resulting effects on the stream environment. The model is capable of simulating runoff from a highly urbanized watershed with a drainage system of river channels and a sewer network, which enables appropriate prediction of river floods and inflows to wastewater treatment plants. Such a model is designed to investigate factors affecting spatial and temporal variations of the stream temperature by incorporating anthropogenic heat impacts and urban canopy processes. By applying the model to the Kanda River Watershed in Tokyo, Japan, stream flow and temperature as well as inflows to a WWTP were simulated well. The anthropogenic heat impact on stream temperature was found to be very significant in winter.

INTRODUCTION

Streams are thought to have important natural functions such as natural landscaping, conserving habitats, and controlling the micro-climate in urban environments. Such functions can be effective when appropriate stream temperatures and other quality levels are maintained. However, urban streams are vulnerable to thermal pollution due to various direct and indirect anthropogenic impacts such as the effluent from wastewater treatment plants, destruction of riparian vegetation, river channelization, the runoff from paved surfaces and global warming. Increased stream temperature can decrease the environmental importance of urban streams and various ecological impacts have been observed such as the increase in invasive species. Because of increasing urban water and energy waste due to population growth and high energy consumption life-styles, the temperature and magnitude of urban wastewater has increased significantly (Kinouchi, 1), which may have resulted in the long-term increase in stream temperature. Kinouchi et al. (2)

indicated that the stream temperature in winter and early spring in the central Tokyo increased at a rate of 0.11 – 0.21 °C/year in river segments that had a considerable increase in wastewater heat input.

To conserve environmental values of urban streams, a framework needs to be provided for predicting stream temperatures under various natural and anthropogenic controlling factors. Although there are many physically based in-stream models that are capable of simulating the shading effects (Sinokrot and Stefan, 3), the impact of urbanization (LeBlanc et al., 4) and global warming (Tung et al., 5), few studies have modelled and validated stream temperature variations considering hydrological processes in a watershed scale (Chen et al., 6; Haag and Luce, 7). However, the predictive framework of urban stream temperature needs to include hydrological modeling as the stream temperature is very dependent on the hydrological behavior of watersheds as well as on the riparian conditions and anthropogenic heating/cooling factors. In addition, characteristic radiation environment in channels run through highly urbanized areas requires special modeling of air-water heat fluxes. For this purpose, a physically based distributed hydrological model developed by Jia et al. (8~10) was coupled with a newly developed model of heat transport in river water, and the performance of the model was demonstrated by applying it to a highly urbanized watershed in Tokyo, Japan, where anthropogenic impacts are significant in modifying natural hydrologic cycle and the water temperature.

MODEL

Modeling hydrological system with dual drainage networks

The simulation of hydrological processes in an urbanized watershed with dual drainage system is based on the WEP model, a physically based distributed hydrological model developed by Jia et al. (8~10). The main features of this model include coupling simulation of hydrological processes and energy transfer processes, simulation of interactive impact of surface water and groundwater, and the mosaic structure within a grid cell. The simulated hydrological processes include evapotranspiration, infiltration, surface runoff, subsurface runoff, groundwater flow, overland flow, and river flow. The simulated energy transfer processes include short-wave radiation, long-wave radiation, latent heat flux, sensible heat flux, and soil heat flux.

In urbanized watersheds equipped with sewer networks, storm runoff flows down through gutters, lateral pipes and sewer pipes during periods of rainfall. In a combined sewer system, the stormwater mixed with waste from houses and buildings eventually flows into a wastewater treatment plant (WWTP). Untreated wastewater in the sewer system overflows to a river system through combined sewer overflow (CSO) outlets following heavy rainfalls. In no-rainfall periods, the waste water from houses and buildings flows into the WWTP and the treated wastewater is discharged into streams. To take these characteristics of dual drainage networks into account in the WEP model, flows in sewer pipes are routed as an overland flow in underground spaces, instead of directly solving unsteady flows in a sewer network, to reduce modeling complexity. Overland flow routing is carried out by means of the kinematic wave method with equivalent roughness parameters deduced from land use data, while a single value is given for the flow routing in a sewer network.

The magnitude of CSO depends on the structure and dimension of the CSO outlet and the water level within the CSO outlet. As this model does not predict water levels in the CSO outlet, we alternatively modeled flows at the CSO outlet by setting the maximum capacity of stormwater inflows to the WWTP as follows:

$$Q_{of}{}^{j} = Q_{in}{}^{j} - Q_{lm}{}^{j}, \quad Q_{lm}{}^{j} = V_{lm} CA_{j} / CA \tag{1}$$

where Q_{of}^{j} = the overflow to the river from the CSO outlet j, Q_{in}^{j} = the inflow to a computational mesh where the CSO outlet j is located, Q_{lm}^{j} = the outflow to a downstream computational mesh from the mesh where the CSO outlet j is located, V_{lm} = the maximum inflow capacity at the WWTP, CA = upstream catchment area of the WWTP, CA_j = the catchment area at CSO outlet j. V_{lm} is given by $V_{lm} = \beta V_{TP}$, where V_{TP} is the treatment capacity of the WWTP, β is a constant. In practice, common sewer design allows inflow three times larger than the designed magnitude, which means $\beta = 3$. However, β could be different from the design setting in reality, thus β is a calibration factor in this study.

Sewerage from houses and buildings during periods without rainfall is routed to compute inflows to the WWTP. The flow routing in a sewer network considers the seepage of groundwater and soil moisture into sewer pipes. The soil moisture seepage is modeled so that it is proportional to the unsaturated conductivity in the ground, and the seepage of the groundwater depends on the level difference of groundwater table and the water level in a pipe.

Modeling heat transport in streams

A basic equation for heat transport in an open channel is written as

$$\frac{\partial(AT)}{A\partial t} + \frac{\partial(QT)}{A\partial x} = \frac{1}{A}\frac{\partial}{\partial x}(AD\frac{\partial T}{\partial x}) + \frac{W_h}{\rho_w c_{pw} V} + \frac{J_h}{\rho_w c_{pw} H} + \frac{J_s}{\rho_w c_{pw} H} \tag{2}$$

where T = the water temperature [°C]; A = the cross-sectional area [m^2]; Q = the flow rate [m^3/s]; D = the longitudinal dispersion coefficient; W_h = the net heat load from surface flow, subsurface flow, groundwater flow, treated wastewater and combined sewer overflow [J/s]; J_h = the air-water heat flux [W/m^2]; J_s = the heat flux from the stream bed to the stream water [W/m^2]; V = the water volume of stream element [m^3]; H = the water depth [m]; ρ_w = the density of water [kg/m^3]; c_{pw} = the specific heat of water [J/kg/°C]; x = the flow direction [m]; t = the time [s]. The net heat load W_h from sources is computed as

$$W_h = \rho_w c_{pw}(\sum Q_{ps} T_{ps} + \sum Q_{nps} T_{nps}) \tag{3}$$

where Q_{ps} and T_{ps} are the magnitude and temperature of point source (wastewater effluents from WWTPs and CSO), respectively; Q_{nps} and T_{nps} represent the magnitude and temperature of non-point source (surface flow, subsurface flow and groundwater flow), respectively. Thermal runoff may cause a rise of stream temperature to a lethal level during rainfall periods in hot seasons (Herb et al, 11). However, since we mainly focus on stream temperature variations during the low flow periods, the temperature of the surface runoff is assumed to be the same as the air temperature. The observed volume and temperature of the wastewater effluents were used, though it can be computed from Kinouchi (1). The temperature of subsurface and groundwater flows is assumed to be the same as the ground temperature at a specified depth. The ground temperature $T_{gd}(z, t)$ at depth z is computed from equation (4) (Carslaw and Jaeger, 12) with the ground surface temperature given by equation (5).

$$T_{gd}(z,t) = A_0 + \sum_{n=1}^{6} A_n \exp\left(-z\sqrt{n\omega/2a}\right)\sin\left(n\omega t - z\sqrt{n\omega/2a} + \varepsilon_n\right) \tag{4}$$

$$T_{gd}(0,t) = a_0 + \sum_{n=1}^{6}\left[a_n \cos(n\omega t) + b_n \sin(n\omega t)\right] \tag{5}$$

$$A_n = \sqrt{a_n{}^2 + b_n{}^2} \tag{6}$$

where $\sin(\varepsilon_n) = a_n/A_n$; $A_0 = a_0$; $\omega = 2\pi/\tau$; τ = the period; a = the thermal diffusivity; a_n and b_n are the Fourier coefficients.

The air-water heat flux J_h is computed as

$$J_h = RN - J_c - J_e = I_s^* + J_s^* - J_c - J_e \tag{7}$$

where RN = the net radiation at the water surface; J_c = the sensible heat flux; J_e = the latent heat flux; I_s^* = the net solar shortwave radiation at the water surface; J_s^* = the net atmospheric longwave radiation at the water surface. The net radiation RN is associated with many factors such as the solar zenith angle, the river transversal and cross-sectional dimensions, riparian vegetation and buildings. Here, we take such factors into account, except for the shading effect of buildings.

The net solar shortwave radiation I_s*, I_w* and the net atmospheric longwave radiation J_s*, J_w* are given as

$$\begin{aligned} I_s^* = {} & S_{DIR}(w-L)(1-\alpha_s)/w + S_{DIF}\psi_s(1-\alpha_s) + S_{DIR}L\alpha_w(1-\psi_s)(1-\alpha_s)/(2h) \\ & + S_{DIF}\psi_w(1-\psi_s)\alpha_w(1-\alpha_s) \end{aligned} \tag{8}$$

$$\begin{aligned} I_w^* = {} & S_{DIR}L(1-\alpha_w)/(2h) + S_{DIF}\psi_w(1-\alpha_w) + S_{DIR}(w-L)\psi_w\alpha_s(1-\alpha_w)/w + S_{DIF}\psi_w(1-\alpha_w) \\ & + S_{DIR}L(1-2\psi_w)\alpha_w(1-\alpha_w)/(2h) + S_{DIF}\psi_w(1-2\psi_w)\alpha_w(1-\alpha_w) \end{aligned} \tag{9}$$

$$J_s^* = \psi_s\varepsilon_s L\downarrow + (1-\psi_s)\varepsilon_s\varepsilon_w\sigma T_w^4 - \varepsilon_s\sigma T^4 \tag{10}$$

$$J_w^* = \psi_w\varepsilon_w L\downarrow + \psi_w\varepsilon_w\varepsilon_s\sigma T^4 + (1-2\psi_w)\varepsilon_w{}^2\sigma T_w^4 - \varepsilon_w\sigma T_w^4 \tag{11}$$

where subscripts s and w denote the water surface and the river side wall, respectively, S_{DIR} and S_{DIF} are downward direct and diffuse solar radiations on a horizontal surface at the top of a stream channel canopy, $L\downarrow$ = the downward atmospheric longwave radiation; ψ_s = the sky-view factor for the water surface; ψ_w = the sky-view factor for one side wall; T_w = the surface temperature of the river side wall; h = the channel depth; w = the channel width; L = the shadow length; ε_s and ε_w are the emissivity of the water surface and the river side wall, respectively, α_s and α_w are the albedo of the water surface and the river side wall, respectively, σ = the Stefan–Boltzmann constant.

The sky-view factors of the water surface ψ_s and the river wall ψ_w are given from Masson (13) as

$$\psi_s = \left[(\mathrm{h}/w)^2 + 1\right]^{1/2} - \mathrm{h}/w \tag{12}$$

$$\psi_w = \frac{1}{2}\left\{\mathrm{h}/w + 1 - \left[(\mathrm{h}/w)^2 + 1\right]^{1/2}\right\}/(\mathrm{h}/w) \tag{13}$$

The shadow length L is computed as (Kusaka et al., 14)

$$L = \begin{cases} h \tan\theta_z \sin\theta_n & (\mathrm{L} < w) \\ w & (\mathrm{L} \geq w) \end{cases} \tag{14}$$

where θ_z = the solar zenith angle; θ_n = the difference between the solar azimuth angle and the stream channel orientation.

The riparian vegetation and structures crossing the stream modify the shortwave and longwave radiative fluxes. We modelled the attenuation of the solar radiation by the riparian vegetation as follows:

$$S_{DIR} = f_s SDIR \tag{15}$$

$$S_{DIF} = f_s SDIF \tag{16}$$

$$f_s = 1 - \lambda I_{veg} f_{LAI} \tag{17}$$

$$f_{LAI} = (LAI - L_{\min}) / (L_{\max} - L_{\min}) \tag{18}$$

where f_s = an attenuation factor for the riparian vegetation, *SDIR* = direct solar radiation at the above-canopy level; *SDIF* = diffuse solar radiation at the above-canopy level; I_{veg} = a riparian vegetation index (0 : no vegetation, 1 : vegetation along one side, 2 : vegetation along both sides); *LAI* = the leaf area index of the riparian vegetation; L_{max} = maximum value of *LAI*; L_{min} = minimum value of *LAI*; λ = a calibrated constant to reflect the shading effect by riparian vegetation.

The sensible heat flux is expressed as (Chapra et al., 15)

$$J_c = c_1 f(u)(T - T_a) \tag{19}$$

where $c_1 = 0.47$; $f(u) = 19 + 0.95u^2$; T_a = the air temperature (°C); u = the wind speed at a height of 7 m (m/s). The incoming radiations at the above-canopy level (*SDIR*, *SDIF* and $L\downarrow$) and the latent heat flux in equation (7) are computed by Jia et al. (8).

The heat flux from the river bed to the stream water (J_s) is calculated from equations (20) through (22).

$$J_s = \rho_{sed} c_{ps} \frac{2\alpha_{sed}}{H_{sed}} (T_{sed} - T) \tag{20}$$

$$\frac{dT_{sed}}{dt} = k_h (T - T_{sed}) \tag{21}$$

$$k_h = 2\alpha_{sed} / {H_{sed}}^2 \tag{22}$$

where T_{sed} = the temperature of the river bed layer; H_{sed} = the effective thickness of the river bed layer; ρ_{sed} = the density of the river bed layer; c_{ps} = the specific heat of the river bed layer; α_{sed} = the thermal diffusivity of the river bed layer.

The surface temperature of the river side wall (T_w) is calculated by a similar formulation using equations (23) through (27).

$$J_w^* + I_w^* = H_C + G_C \tag{23}$$

$$\frac{dT_g}{dt} = k_{hg}(T_w - T_g) \tag{24}$$

$$H_C = c_1 f(u)(T_w - T_a) \tag{25}$$

$$G_C = \rho_g c_{pg} \frac{2\alpha_g}{H_g}(T_w - T_g) \tag{26}$$

$$k_{hg} = 2\alpha_g / H_g^{\,2} \tag{27}$$

where H_C = the sensible heat flux from the river side wall; G_C = the heat flux from the river side wall into the ground; H_g = the thickness of the river side wall; T_g = the internal temperature of the side wall; ρ_g = the density of the side wall; c_{pg} = the specific heat of the side wall; α_g = the thermal diffusivity of the side wall.

A discrete form of equation (2) is written by equation (28) after Chapra et al. (15). Equation (28) is implicitly solved by means of the Gaussian elimination method.

$$\begin{aligned}\frac{dT_i}{dt} = {} & \frac{Q_{i-1}}{V_i}T_{i-1} - \frac{Q_i}{V_i}T_i + \frac{D'_{i-1}}{V_i}(T_{i-1} - T_i) + \frac{D'_i}{V_i}(T_{i+1} - T_i) \\ & - \frac{1}{A_i}\frac{dA_i}{dt}T_i + \frac{W_{h,i}}{\rho_w c_{pw} V_i} + \frac{J_{h,i}}{\rho_w c_{pw} H_i} + \frac{J_{s,i}}{\rho_w c_{pw} H_i}\end{aligned} \tag{28}$$

$$D'_i = D_i \cdot A_i / (\Delta x_i + \Delta x_{i+1}) / 2 \tag{29}$$

where subscript i denotes river element i, Δx = the length of river element i.

APPLICATION

Study area

We applied the hydrological model coupled with the heat energy transport model to the Kanda River watershed located in the heart of Tokyo, Japan (Figure 1). Tributaries run in four open channels and one covered channel in upstream sub-watersheds, and eventually merges to the mainstream. The Momozono River is a covered channel all along the stream (Figure 1). The channels have a trapezoidal cross-sectional shape in most of their reaches, some of which have a small ditch on the bottom of the channel. The Kanda River watershed has a combined sewer system and the watershed can be divided into five sewer catchments. Sewage generated in the catchment bounded by a dashed line (Figure 1) flows

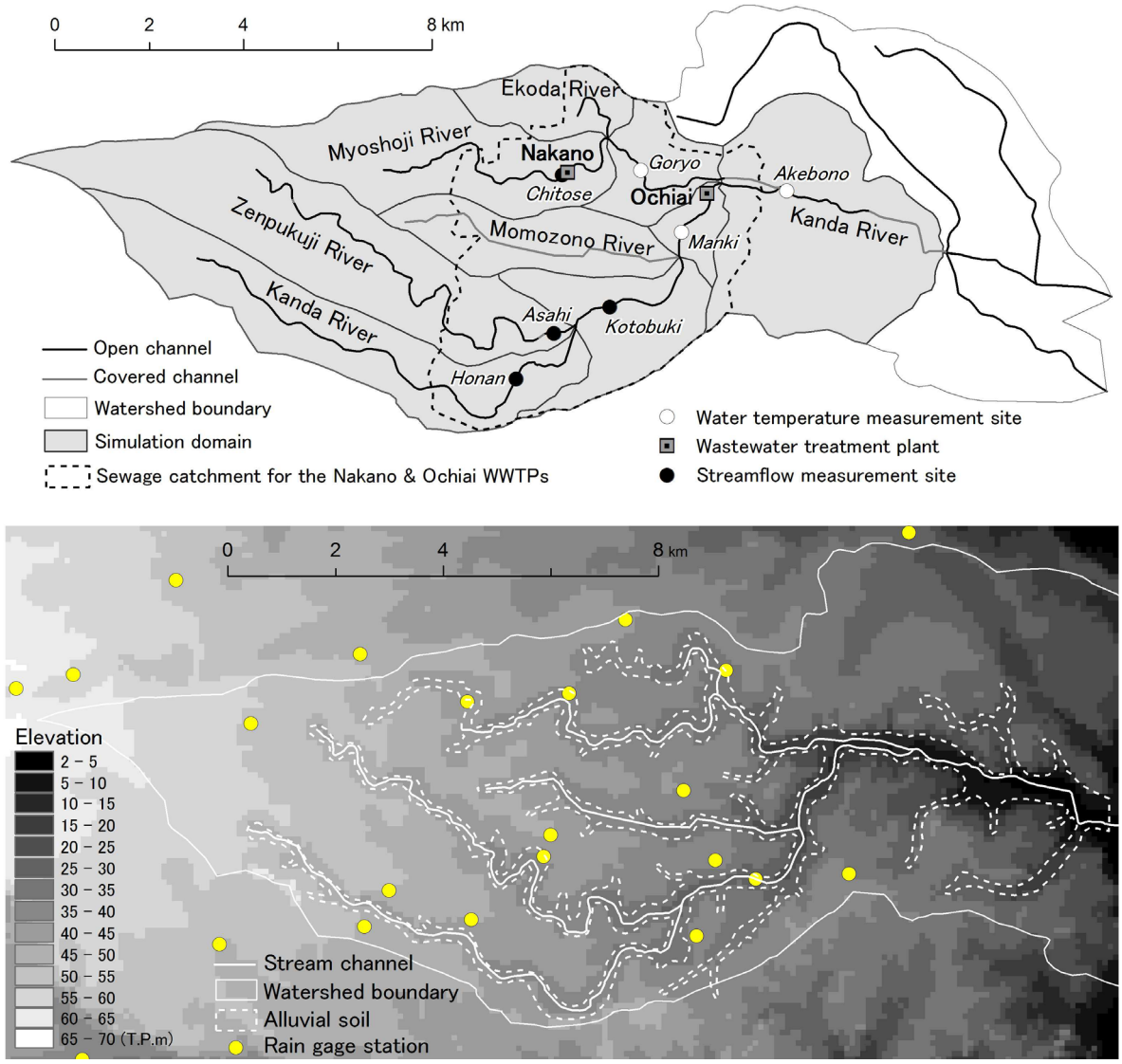

Figure 1. Outline of the Kanda Watershed

into two WWTPs within the watershed (the Ochiai WWTP and the Nakano WWTP), where treated effluents are discharged into the Kanda River. In all other catchments, the sewage is transported to WWTPs located outside the Kanda River watershed through the sewer pipes across the watershed boundary. Stormwater flows in the same route during periods of rainfall with relatively light intensity. During periods of heavy rainfall, the CSO in all sewer catchments directly discharges into the Kanda River system from the CSO outlets located within the watershed.

Input data and parameters

The main input data required to run the model are listed in Table 1. Spatial distribution of correspondent data was prepared using ArcGIS. Stream network data was reproduced on the GIS platform from the digital maps by the Geographical Survey Institute. The watershed was divided into 9 sub-watersheds. River cross-sectional area was approximated as a trapezoidal shape. The shape data was provided by the maps obtained from the Tokyo Metropolitan Government. The orientation of the stream channel was calculated for each river element by utilizing a tool of ArcGIS. Categorized data of riparian vegetation and structures crossing channels, which were prepared from aerial photographs, are attributed to individual computational element of river channels. The actual sewer network data was not used. Instead, we

Table 1. List of main input data used for the coupled model simulation

Category	Item	Source
Land surface conditions	Watershed boundary	National digital information*
	Topography	Digital map* (50m by 50m DEM)
	Land use	Fine digital information* (13 types of land use, 100m by 100m raster data)
	Soil type	Geologic map
Meteorological and hydrological conditions	Precipitation (19 stations)	Hourly data from the Tokyo Metropolitan Government
	Relative humidity (1 station)	
	Air temperature (3 stations)	Hourly data from AMeDAS by the Japan Meteorological Agency
	Wind velocity (3 stations)	
	Sunshine duration (3 stations)	
River network and hydraulic dimensions	Stream channel	Digital Map (1:25,000)
	River profiles	Maps obtained from Tokyo Metropolitan Government
	Riparian vegetation	Aerial photographs
	Crossing structure	Aerial photographs
Anthropogenic conditions	Population	National census data by the Ministry of Internal Affairs and Communications
	Sewer catchment boundary	Maps obtained from the Tokyo Metropolitan Government

*Products of the Geographic Survey Institute

Table 2. Parameters used for the heat transport model

parameters	River bed	River side wall
Thickness H_{sed}, H_g (m)	0.1	0.3
Density ρ_{sed}, ρ_g (g/cm^3)	2.2	2.4
Specific heat c_{ps}, c_{pg} (cal/g/K)	0.21	0.21
Thermal diffusivity α_{sed}, α_g (cm^2/s)	0.008	0.02
Albedo α_s, α_w	0.08*	0.3
Emissivity ε_s, ε_w	0.95*	0.90

*Values for water surface

assumed that the flows in the sewer pipes followed the terrain of the watershed, which was found to be a reasonable assumption.

There are three categories of parameters used in the WEP model (Jia et al., 8~10): (1) parameters of land surface and river channel system; (2) parameters of vegetation; and (3) parameters of soil and aquifer. Parameters for the heat transport model are additionally specified following Chapra et al. (15) and Oke (16) as listed in Table 2. All of parameters were initially specified from literatures or estimated according to land cover information, observation data, and some parameters are selected for model calibration. The model calibration was performed for both stream flows and temperatures at locations where observed values are obtained. For flow simulations, some flood hydrographs and low flows were checked to calibrate parameters such as the Manning's roughness of the river flow, β in equation (1) and the hydraulic conductivity of the riverbed. Parameter β used to give V_{lm} in equation (1) was set to 5 following the calibration. Calibration of parameters for the stream temperature including λ in equation (17) was carried out to reproduce its seasonal and diurnal variations. Ratios of the impervious area, four types of pervious areas and water surfaces for each computational mesh (100m by 100m) were given by reclassifying the fine land use data using the parameters in Table 3, which were deduced referring to previous studies (Jia et al., 9 and 10).

The spatial distribution data of the topsoil was generated from geological maps. The topsoil in the watershed is

Table 3. Land use classification parameters

Land use type of the fine digital information	Land use classification used in the WEP model						
	Water surface ratio	Pervious area (PA)				Impervious area (IA)	
		Paddy ratio in PA	Tall vegetation ratio in PA	Short vegetation ratio in PA	Bare soil ratio in PA		Urban canopy rate in IA
forest	0	0	0.8	0.2	0	0.27	0
paddy	0	1	0	0	0	0	0
other farmland	0	0	0.2	0.8	0	0.21	0
under preparing	0	0	0.2	0.3	0.5	0.23	0
vacant land	0	0	0.2	0.3	0.5	0.27	0
industrial use	0	0	0.2	0.3	0.5	0.75	0.36
housing area	0	0	0.2	0.3	0.5	0.75	0.36
housing area	0	0	0.2	0.3	0.5	0.75	0.36
commercial area	0	0	0.2	0.3	0.5	0.80	0.36
road	0	0	0	1	0	0.86	0
park	0	0	0.3	0.5	0.2	0.16	0.36
public works	0	0	0.2	0.3	0.5	0.45	0.36
river/lake	1	0	0	0	0	0.14	0

mainly the Kanto loam, except for the alluvial soil in riparian zones (Figure 1). The physical properties for each soil type such as soil porosity, soil saturated hydraulic conductivity and soil moisture–suction relation curve were given from Jia et al. (9 and 10). Values of Manning's roughness coefficient for river flow and overland flow were set to 0.015 and 0.01, respectively. The air-water heat flux in the Momozono river, a fully covered channel, was computed by setting the direct and diffuse solar radiations as zero and the downward longwave radiation from the cover was assumed to be the same as $L\downarrow$.

Model application

The coupled model was run for the simulation from January 1 to December 31 of 2005 in a time step of 1 hour (except for overland flow and river flow routing with a time step of 10 minutes) and a grid cell size of 100m×100m. The computational domain includes 9062 grid cells. River channels were divided into computational elements with the longitudinal length of 390m - 450m. The headwater of the stream was maintained by the pumped groundwater. Thus, the upstream boundary conditions were set by the constant stream flow and variable water temperatures deduced from the ground temperature. The temperature of the base flow from the groundwater was likewise set at an equivalent temperature of the ground at the depth of the river bed.

Results

Streamflow and inflow to WWTPs

The simulated results of low streamflows were compared with those observed at Kotobuki and Chitose (Figure 1,

Table 4. Comparisons of simulated stream flow with observed during no-rainfall periods

Location	Period	Observed average flow	Simulated average flow
Kotobuki	2005/1/20-21	0.52 m^3/s	0.55 m^3/s
Chitose	2005/1/18-19	0.07 m^3/s	0.10 m^3/s

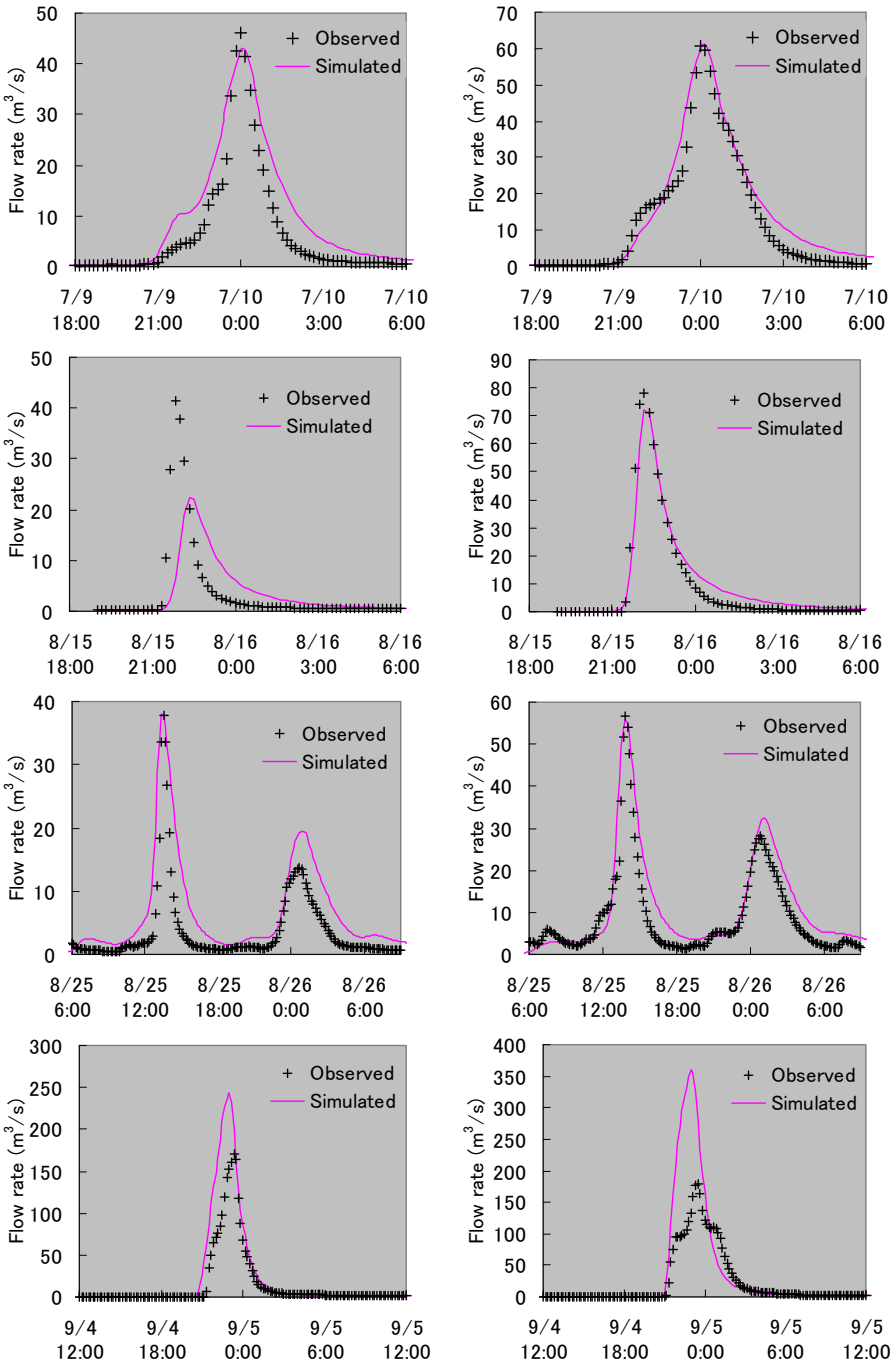

Figure 2. Comparison of simulated flood discharges with observed (left: Honan, right: Asahi)

Table 4). Most of the river reaches are covered by a concrete bottom slab and side walls, which prevent water interaction between river flows and groundwater. As a result, the streamflow could be quite low during periods without rainfall. This situation was reproduced well by the simulation. Simulated flood discharges during four major storm events in 2005 were compared with hydrographs at Asahi and Honan obtained from observed rating curves and measured water levels. Simulated hydrographs relatively well reproduced observed ones at Asahi for three events (July 9-10, August 15-16 and

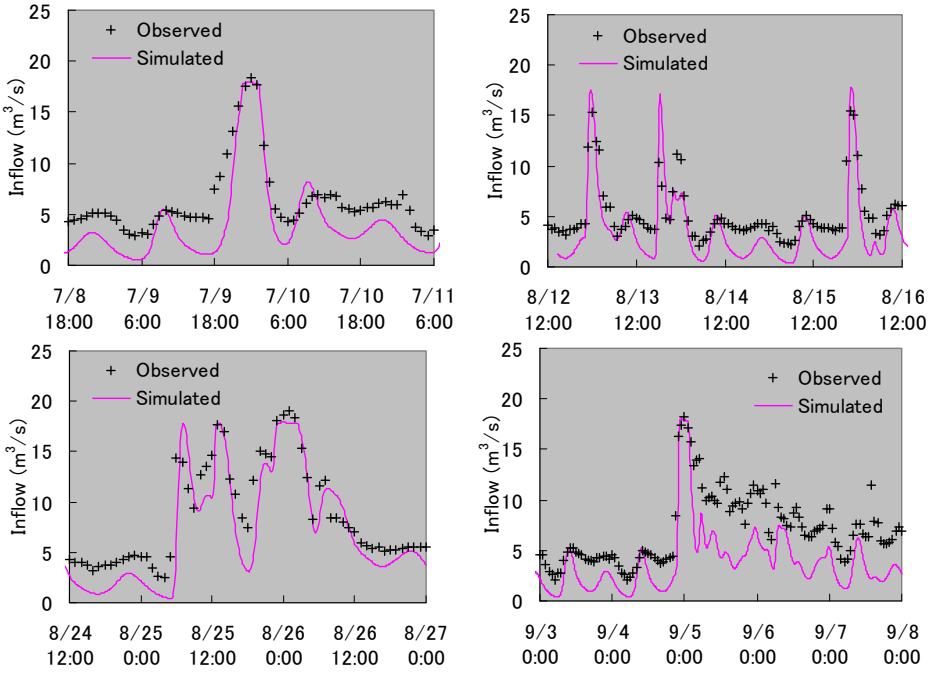

Figure 3. Comparison of simulated inflows to the Ochiai WWTP during four rainfall events

August 25-26) and at Honan for two events (July 9-10 and August 25-26) as shown in Figure 2. Most abrupt changes of discharge were observed during the rainfall event of August 25-26, in which the water level rose about 1.5m within 40 minutes. Similar features are simulated for this event even though hourly rainfall data are used. Simulated hydrographs for rainfall periods from September 4 to 5, which was caused by the approach of the typhoon No.14, overestimated the peak discharge and the total volume at both locations. During this period, flooding occurred along the stream channels and the runoff was temporally stored in detention reservoirs located upstream of the watershed, while the model does not deal with these processes. Figure 3 shows the correspondent inflows to the Ochiai WWTP. Diurnal variations and abrupt changes of the inflow were simulated well, although the simulated base inflows underestimated measured ones probably due to the setting of the seepage modeling. Our observations showed that the seepage accounts for about 20% of the total inflow to the WWTPs in Tokyo (Nakayama et al., 17). Therefore, further verifications may be needed for the modeling of soil-water seepage from the ground surrounding the sewer pipes.

Water temperature

The simulated stream temperatures are compared with those observed (Figure 4). Modeled stream temperatures matched well with those observed at Goryo throughout the year. Modeled stream temperatures at Manki show larger amplitudes of the diurnal variation than those observed in the fall and winter seasons. Akebono, where we started temperature measurement from November 2005, exhibited flatter temperature variations than those observed at Goryo and Manki. This is mainly because the wastewater effluents from two WWTPs comprise the main portion of the streamflow at Akebono and thus the diurnal temperature variation is dominated by the effluent temperature that has small diurnal amplitudes. In addition, our monitoring detected sudden descends of the stream temperature at Akebono, followed by the soon recovery to the previous temperature level. For example, the phenomenon occurred in the morning of the 23rd of November, probably due to the temporal reduction in wastewater effluents to 0.8m^3/s from its daily average of 2.1m^3/s. These abrupt temperature changes at Akebono were also well captured by the simulation (Figure 4). Stream

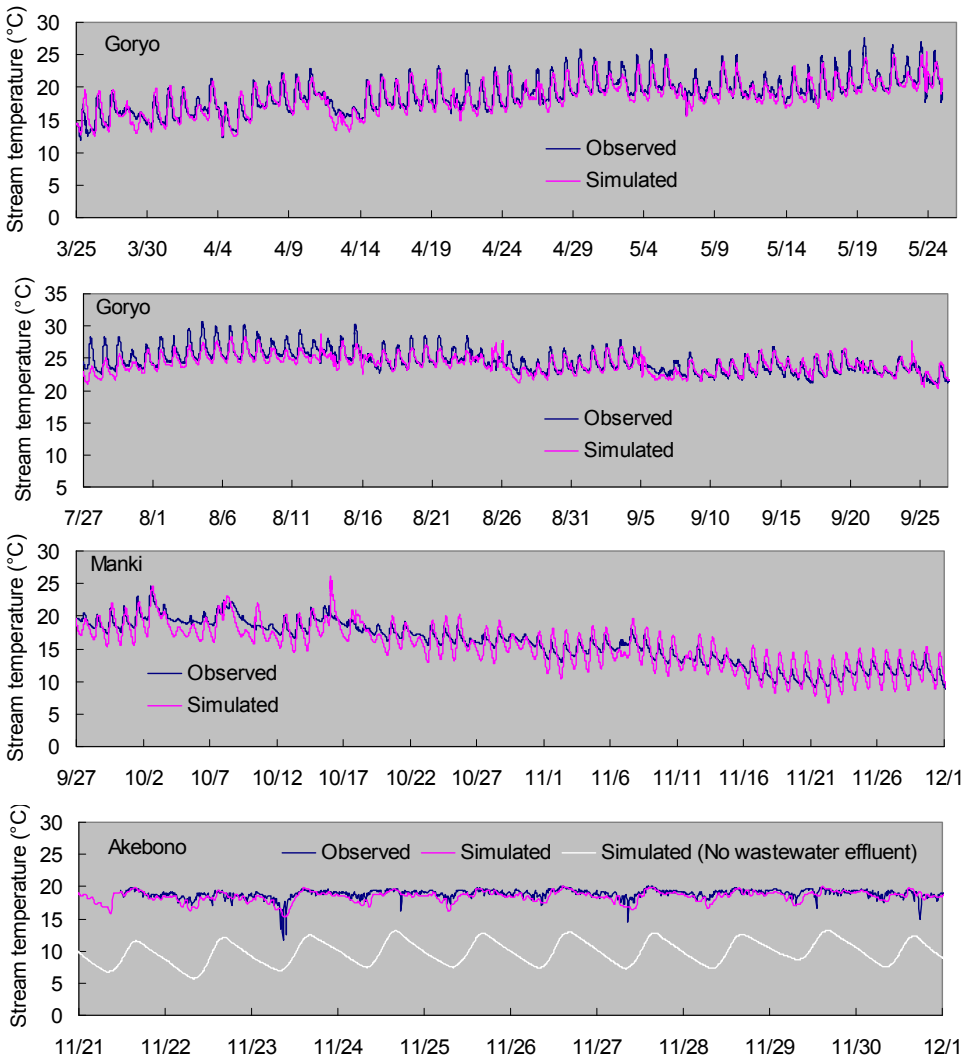

Figure 4. Comparison of simulated stream temperatures with observed

The bottom figure includes results for the hypothetical case of no wastewater effluent.

temperatures simulated by assuming no wastewater inputs were far below the temperatures simulated with wastewater inputs (Figure 4, bottom), and the maximum difference of stream temperature was found to be approximately 12°C. This suggests that there is a strong influence of wastewater effluents on the stream temperature in the Kanda River, and potential impacts on the habitat for fish and invertebrates and algae growth.

CONCLUSIONS

A framework was presented for the stream temperature prediction under distributed anthropogenic and natural heat sources in the urbanized watershed. The predictive model developed in this study is based on a model of heat transport in river water incorporated into a physically based distributed hydrological model (WEP model). This coupled model can simulate dynamic hydrological responses of an urbanized watershed with a drainage system of river channels and a combined sewer network, which enables appropriate prediction of inflows to wastewater treatment plants and streamflows. Stream temperature prediction considers the influence of heat input by wastewater effluents, groundwater seepage, surface runoff as well as the atmospheric radiations, and the heat budget within a river canopy. This model was applied to the Kanda River watershed in Tokyo, and showed that it could reproduce well low flows and flood runoff, including inflows to

the WWTP. Overall magnitudes of the simulated stream temperature agreed well with those of observed. Impacts of anthropogenic heat input from WWTPs were found to be very significant in winter. Abrupt changes of stream temperature in a time scale of several hours were attributed to the fluctuation of the volume of wastewater effluents. Further improvements are necessary to more accurately simulate observed seasonal and diurnal variations in the stream temperature throughout the year.

ACKNOWLEDGMENTS

This research project was financially supported by CREST (Core Research for Evolutional Science and Technology) of the Japan Science and Technology Corporation as a part of the research project 'Water and Energy Forcing due to Urbanization in Land-Atmosphere-Coastal System' organized by Prof. Manabu Kanda (Tokyo Institute of Technology).

REFERENCES

1. Kinouchi, T.: Impact of long-term water and energy consumption in Tokyo on wastewater effluent: implication for thermal degradation of urban streams, Hydrological Processes, Vol.21, pp.1207 - 1216, 2007.
2. Kinouchi, T., Yagi, H. and Miyamoto, M.: Increase in stream temperature related to anthropogenic heat input from urban wastewater, Journal of Hydrology, Vol.335, pp.78-88, 2007.
3. Sinokrot, B.A. and Stefan, H.G.: Stream temperature dynamics: measurement and modeling, Water Resources Research, Vol.29, No.7, pp.2299–2312, 1993.
4. LeBlanc, R.T., Brown, R.D. and FitzGibbon, J.E.: Modeling the effects of land use change on the water temperature in unregulated urban streams, Journal of Environmental Management, Vol.49, pp.445–469, 1997.
5. Tung C., Lee T. and Yang Y.: Modelling climate change impacts on stream temperature of Formosan landlocked salmon habitat, Hydrological Processes, Vol.20, pp.1629–1649, 2006.
6. Chen, Y.D., McCutcheon, S.C., Norton, D.J. and Nutter, W.L., Stream temperature simulation of forested riparian areas: II. Model application, Journal of Environmental Engineering, ASCE, Vol.124, No.4, pp.316–328, 1998.
7. Haag, I. and Luce, A., The integrated water balance and water temperature model LARSIM-WT, Hydrological Processes, Vol.22, pp.1046-1056, 2008.
8. Jia, Y., Ni, G., Kawahara, Y. and Suetsugi, T.: Development of WEP model and its application to an urban watershed, Hydrological Processes, Vol.15, No.11, pp.2175-2194, 2001.
9. Jia, Y., Ni, G., Yoshitani, J., Kawahara, Y. and Kinouchi, T.: Coupling simulation of water and energy budgets and analysis of urban development impact, Jour. of Hydrologic Eng., ASCE, Vol.7, No.4, pp.302-311, 2002.
10. Jia, Y., Kinouchi, T. and Yoshitani, J.: Distributed hydrologic modeling in a partially urbanized agricultural watershed using water and energy transfer process model. Jour. of Hydrologic Eng., ASCE, Vol. 10. No. 4, pp.253-263, 2005.
11. Herb, W. R., Janke, B., Mohseni, O. and Stefan, H. G.: Thermal pollution of streams by runoff from paved surfaces, Hydrological Process, Vol.22, pp.987 – 999, 2008.
12. Carslaw, H. S. and Jaeger, J.C.: Conduction of heat in solids 2nd edition, Oxford Univ. Press, London, 1959.
13. Masson, V.: A physically-based scheme for the urban energy budget in atmospheric models, Boundary-Layer Meteorology, Vol.94, No.3, pp.357-397, 2000.
14. Kusaka, H., Kondo, H., Kikegawa, Y. and Kimura, F.: A simple single-layer urban canopy model for atmospheric models: comparison with multi-layer and slab models, Boundary-Layer Meteorology, Vol.101, No.3, pp.329-358, 2001.

15. Chapra, S.C., Pelletier, G.J. and Tao, H.: QUAL2K: A modeling framework for simulating river and stream water quality, version 2.04: documentation and users manual, Civil and Env. Eng. Dept., Tufts University, Medford, MA., 2006.
16. Oke, T.: Boundary Layer Climates 2nd edition, Routledge, New York. 1987.
17. Nakayama, Y., Kanda, M. and Kinouchi, T.: The investigation of the water and heat transfer in urban sewage system based on the temperature observation at the wastewater treatment plants, Journal of Japan Society of Hydrology and Water Resources, Vol.20, No.1, pp.25-33, 2007. (In Japanese)

APPENDIX – NOTATION

The following symbols are used in this paper.

a = thermal diffusivity;

a_n, b_n = the Fourier coefficients;

c_{pg} = specific heat of the side wall;

c_{ps} = specific heat of the river bed layer;

c_{pw} = specific heat of water;

f_s = an attenuation factor for the riparian vegetation;

h = channel depth;

t = time;

u = wind speed at a height of 7 m;

w = channel width;

x = flow direction;

z = depth from the ground surface;

A = cross-sectional area;

CA = upstream catchment area of the WWTP;

CA_j = catchment area at CSO outlet j;

D = longitudinal dispersion coefficient;

G_C = heat flux from the river side wall into the ground;

H = water depth;

H_C = sensible heat flux from the river side wall;

H_g = thickness of the river side wall;

H_{sed} = effective thickness of the river bed layer;

I_s^* = net solar shortwave radiation at the water surface;

I_w^* = net solar shortwave radiation at the river side wall;

J_c = sensible heat flux;

J_e = latent heat flux;

J_h = air-water heat flux;

J_s = heat flux from the stream bed to the stream water;

J_s^* = net atmospheric longwave radiation at the water surface;

J_w^* = net atmospheric longwave radiation at the river side wall;

I_{veg} = riparian vegetation index (0 : no vegetation, 1 : vegetation along one side, 2 : vegetation along both sides);

L = shadow length;

LAI = leaf area index of the riparian vegetation;

L_{max} = maximum value of LAI;

L_{min} = minimum value of LAI;

$L\downarrow$ = downward atmospheric longwave radiation;

Q = flow rate;

$Q_{in}^{\ j}$ = inflow to a computational mesh where the CSO outlet j is located;

$Q_{lm}^{\ j}$ = outflow to a downstream computational mesh from the mesh where the CSO outlet j is located;

Q_{nps} = magnitude of non-point source (surface flow, subsurface flow and groundwater flow);

$Q_{of}^{\ j}$ = overflow to the river from the CSO outlet j;

Q_{ps} = magnitude of point source (wastewater effluents from WWTPs and CSO);

RN = net radiation at the water surface;

$SDIF$ = diffuse solar radiation at the above-canopy level;

S_{DIF} = downward diffuse solar radiation on a horizontal surface at the top of a stream channel canopy;

$SDIR$ = direct solar radiation at the above-canopy level;

S_{DIR} = downward direct solar radiation on a horizontal surface at the top of a stream channel canopy;

T = water temperature;

T_a = air temperature;

T_g = internal temperature of the side wall;

$T_{gd}(z, t)$ = ground temperature at depth z and time t;

T_{nps} = temperature of non-point source (surface flow, subsurface flow and groundwater flow);

T_{ps} = temperature of point source (wastewater effluents from WWTPs and CSO);

T_{sed} = temperature of the river bed layer;

T_w = surface temperature of the river side wall;

V = water volume of stream element;

V_{lm} = maximum inflow capacity at the WWTP;

V_{TP} = treatment capacity of the WWTP;

W_h = net heat load from hydrological sources;

α_g = thermal diffusivity of the side wall;

α_s = albedo of the water surface;

α_{sed} = thermal diffusivity of the river bed layer;

α_w = albedo of the river side wall;

β = a calibrated constant to compute V_{lm};

ε_s = emissivity of the water surface;

ε_w = emissivity of the river side wall;

λ = a calibrated constant to reflect the shading effect by riparian vegetation;

θ_n = difference between the solar azimuth angle and the stream channel orientation;

θ_z = solar zenith angle;

ρ_g = density of the side wall;

ρ_{sed} = density of the river bed layer;

ρ_w = density of water;

σ = the Stefan–Boltzmann constant;

ψ_s = sky-view factor for the water surface;

ψ_w = sky-view factor for one side wall;

Δx = length of a river element.